Cell. Mol. Life Sci. 65 (2008) 991 – 1004
1420-682X/08/060991-14
DOI 10.1007/s00018-008-7526-3

Cellular and Molecular Life Sciences

Research Article

Transient cytoskeletal alterations after SOD1 depletion in neuroblastoma cells

P. Vigilanza[a, †], K. Aquilano[b, †], G. Rotilio[a, b] and M. R. Ciriolo[a, b, *]

[a] Department of Biology University of Rome "Tor Vergata", Via della Ricerca Scientifica 1, 00133 Rome (Italy), Fax: +39-06-7259-4311, e-mail: ciriolo@bio.uniroma2.it
[b] Research Center, IRCCS San Raffaele, Via dei Bonacolsi snc, 00163, Rome (Italy)

Received 15 November 2007; received after revision 19 January 2008; accepted 22 January 2008
Online First 1 February 2008

Abstract. We have studied the effects of superoxide production after Cu,Zn superoxide dismutase (SOD1) down-regulation by RNA interference. We demonstrated that SOD1 depletion induced, only in neuroblastoma cells, a decrease in actin and β-tubulin content and accumulation of neurofilament light chain and Tau proteins. Alterations of cell morphology and the microfilament network were also observed, together with the up-regulation of the Cdk5/p35 pathway, which is involved in the regulation of actin polymerization. The decrease of filamentous actin was transient and was recovered through the activation of p38/Hsp27 MAPK pathway, as well as after treatment with *N*-acetyl-L-cysteine. The importance of p38 in the recovery of cytoskeleton was confirmed by experiments carried out in the presence of its inhibitor SB203580, which induced cell death. Our data demonstrate that SOD1 is essential for the preservation of cytoskeleton integrity, by maintaining physiological concentration of reactive oxygen species and inhibiting the activation of the neuronal specific Cdk5/p35 pathway.

Keywords. SOD1, cytoskeleton, actin, p38/Hsp27, Cdk5/p35.

Introduction

Reactive oxygen species (ROS), when produced at high rate, are able to exert toxic effects on cellular biomolecules. However, the eligible cellular targets of ROS are variable depending on many factors including: (i) cell-specific antioxidant pattern, (ii) intensity and nature of the stress imposed (*e.g.*, radical *versus* non-radical oxidant), and (iii) site of generation (*e.g.*, intra- *versus* extracellular). Due to its structure, cytoskeleton may represent one of the preferential targets of ROS whatever oxidative stress is applied; indeed, cytoskeletal proteins are particularly abundant within the cells and several protein constituents of cytoskeleton display highly reactive residues that can be easily oxidized. It has been demonstrated that oxidative stress causes both microfilament and microtubule disruption essentially due to oxidative modifications of specific methionine and cysteine sulfhydryls of actin and tubulin [1–7]. In particular, exposure of cells to ROS-generating agents (*e.g.*, menadione, diamide, *tert*-butyl hydroperoxide) results in disruption of the normal organization of microfilaments that coincides with a preferential oxidation of the conserved Cys374 of actin [1, 8–10]. More recent evidence indicates that also oxidation in terms of carbonylation of protein residues may play a role in loss of cytoskeletal function [3, 11]. ROS may also cause a rise in calcium concentration promoting

† Both authors equally contributed to this work.
* Corresponding author.

dissociation of actin microfilaments and activation of calpains that cleave actin-binding proteins [12].

ROS, besides being direct damaging factors, when produced at high rate, could also take part in the processes governing cell signaling. In this context, they can represent efficient modulators of signaling kinases also implicated in the regulation of cytoskeletal function. Indeed, under ROS challenge, activation of the redox-sensitive mitogen-activated protein kinase (MAPK) p38 leads to Hsp27 phosphorylation, which in turn promotes actin reorganization and resistance to cell death [13, 14]. Moreover, in cells of neuronal origin, the cyclin-dependent kinase 5 (Cdk5), which is responsible for cell migration, actin dynamics and microtubules polymerization, has been demonstrated to be hyperactivated by oxidative stress conditions [15, 16]. Other proteins that are involved in regulation of cytoskeletal dynamics could be modulated by ROS: an example is represented by Rho GTPases that are inhibited by Rac-mediated ROS increase leading to microfilament rearrangement [17].

Among ROS, superoxide anion is the most abundant radical to be physiologically produced, especially at the level of the mitochondrial electron transport chain. Although superoxide is not a powerful oxidant, it can interact with transition metals or nitric oxide to produce the more potent and versatile oxidants hydroxyl radical and peroxynitrite, respectively. Cells have a well-organized and distinctly antioxidant defense system that is able to counteract ROS cytotoxicity; however, oxidative stress takes place when the capacity of cellular antioxidant defense to scavenge ROS is overwhelmed. This condition is not unusual since oxidative unbalance is a feature of many morbidity state and diseases such as ageing, neurodegenerative disorders [18], and inflammatory states [19]. Cells of neuronal origin are particularly susceptible to oxidative damage due to their high oxidative metabolism and the relatively low abundance of antioxidant defense systems. Thus, mitochondrial dysfunction, accumulation of oxidized proteins (particularly those from cytoskeleton), inflammation, and defects of protein clearance are intertwined processes that selectively kill neuronal cells [18].

Copper, Zinc superoxide dismutase (SOD1) represents the primary enzymatic defense against superoxide. It catalyzes the disproportionation reaction of superoxide to oxygen and hydrogen peroxide at the copper ion that is localized in the active site. In mammalian cells, SOD1 is mainly found in cytosol with a smaller fraction in the mitochondrial intermembrane space, nuclei, lysosomes, and peroxisomes [20]. Recently, it has been proposed that SOD1, besides being the primary defense against superoxide, in neuronal cells may exert an anti-apoptotic function by interacting with the mitochondrial protein Bcl-2. SOD1 mutants, typical of familial forms of amyotrophic lateral sclerosis, display an altered capacity to bind Bcl-2, causing its sequestration and commitment to apoptosis [21]. An increased interaction between mutated SOD1 and the cytoskeletal protein actin with respect to the wild-type enzyme has been also demonstrated. In particular, the enhanced interaction of mutated SOD1 with actin causes cytoskeletal changes, suggesting that this enzyme may have an important role in modulation of microfilament structure [22].

In a previous study, we demonstrated that SOD1 is essential for maintenance of mitochondria homeostasis by inhibiting oxidation of mitochondrial proteins; indeed, in neuroblastoma cells, SOD1 depletion causes an early ROS burst and a decrease of the anti-apoptotic protein Bcl-2 concomitantly to loss of transmembrane potential and ATP production [23]. In the present work, we further studied the consequence of SOD1 depletion by RNA interference (RNAi). With this powerful gene-silencing tool we detected a time-dependent, early change in cytoskeleton homeostasis of neuroblastoma cells in terms of microfilament disruption, β-tubulin decrement, tau and neurofilament light chain (NF-L) accumulation. We also found that the transient increase of superoxide concentration was responsible for the activation of the neuron-specific Cdk5/p35 pathway and that cell viability was assured by recovery of microfilament disruption *via* the activation of p38/Hsp27 pathway.

Experimental procedures

Materials. Protease inhibitor cocktail, *N*-acetyl-L-cysteine (NAC), mouse monoclonal, rabbit polyclonal anti-actin, anti-catalase, anti-SOD1, anti-α- and anti-β-tubulin, anti-NF-L (NF-68) were from Sigma (St. Louis, MO, USA). Goat polyclonal anti-actin, rabbit polyclonal anti-SOD1, anti-p38 and anti-p35, goat polyclonal anti-P-Cdk5 and mouse monoclonal anti-Tau were from Santa Cruz Biotechnology (Santa Cruz, CA, USA). Mouse monoclonal anti-Hsp25 and anti-Hsp27 were from StressGen Biotechnologies Corp. (Victoria, Canada). Rabbit polyclonal anti-P-p38 and anti-P-MKK3/6 were from Cell Signaling Technology Inc. (Danvers, MA, USA). IgG (H+L)-HRP-conjugated goat anti-mouse and anti-rabbit secondary antibodies were from Bio-Rad Laboratories (Hercules, CA, USA). TRIzol® Reagent, Platinum Taq polymerase, M-MLV, primers for RT-PCR, Opti-MEM, dihydroethydium (DHE), Alexa Fluor® 488-phalloidin, Hoechst 33342 and Alexa Fluor® 568

goat anti-mouse were from Invitrogen (Carlsbad, CA, USA). siRNA were from Dharmacon (Lafayette, CO, USA). All other chemicals were obtained from Merck (Darmstadt, Germany). p38 inhibitor SB203580 was from Calbiochem (Merck KGaA, Darmstadt, Germany)

Cell cultures and treatments. SH-SY5Y neuroblastoma and gastric adenocarcinoma (AGS) cells were purchased from the European Collection of Cell Cultures. M14 melanoma cells were kindly provided by Dr. Anna Maria Biroccio (Istituto di Ricerca "Regina Elena", Rome, Italy), NSC34 cells (neuroblastoma × spinal cord hybridoma cells) were kindly donated by Dr. Neil R. Cashman (University of Toronto, Canada). CHP100 neuroblastoma cells were kindly provided by Prof. Spinedi (University of Rome "Tor Vergata", Italy). SH-SY5Y cells were grown in Dulbecco's modified Eagle's medium-F12 supplemented with 10% FCS (Gibco, Carlsbad, CA, USA). CHP100 cells were grown in RPMI, AGS were grown in F12 and NSC34 in DMEM media supplemented with 10% FCS, 1% penicillin/streptomycin and 1% glutamine. Cell cultures were maintained at 37°C in an atmosphere of 5% CO2 in air. All media were from Sigma-Aldrich. Inhibition of p38 activity was carried out using the specific SB203580 inhibitor. SB203580 was added at concentration of 20 μM to cell culture medium immediately after transfection. NAC was added at a concentration of 5 mM to cell culture medium immediately after transfection.

Transfections. At 24 h before transfection, cells were seeded at 60% confluence. The day of transfection, cells were trypsinized, and then re-suspended in Opti-MEM® supplemented with 6 mM glucose and 0.11 mM 2-mercaptoethanol and transfected with a 21-nucleotide siRNA duplex (*sisod*) directed against the following SOD1 target sequences: 5′-AAGGCCUGCAUGGAUUCCAUG-3′ (for human SOD1) [23] and 5′-AAAUUACAGGAUUAACUGAAG-3′ (for mouse SOD1). These sequences were determined to be unique, respectively, to the human and mouse *sod1* gene by basic local alignment search tool of GenBank database. The selected siRNA sequence for mouse SOD1 mRNA was chosen among six as it gave a stronger decrease of SOD1 protein. Negative control cells were transfected with a scramble siRNA duplex (*siscr*), which does not present homology with any other human or mouse mRNAs. To prove the specificity of the action of RNAi, a siRNA sequence for lamin A/C was used that was provided by the manufacturer together with SOD1 siRNAs. All the experiments were performed on untransfected cells as additional control. As no difference was detectable between *siscr* and untransfected cells, in the figures we show only the negative control *siscr*. Cells were transfected by elecroporation using a Gene Pulser Xcell system (Bio-Rad) according to the manufacturer's instructions and immediately seeded into fresh medium. Times longer than 48 h were not considered, as a starting recovery of the protein was detected at 60 h. Transfection efficiency of siRNA estimated by co-transfecting siRNAs with non-specific rhodamine-conjugated oligonucleotides was found to be >80%.

Microscopy analysis. Cells were seeded directly on glass coverslips. At each time, cells were fixed with 4% solution paraformaldehyde and then permeabilized with a solution of 0.4% PBS-Triton X-100. Cells were probed with mouse anti-SOD1 antibody diluted (1:200) in blocking solution (PBS/FBS 10%) and then with fluorescent Alexa Fluor® 568 goat anti-mouse antibody (1:1000). Similarly, cells were stained for filamentous actin (F-actin) content with Alexa Fluor® phalloidin-488 (200 nM) and with Hoechst 33342 (10 μg/ml) to visualize nuclei. Appropriate negative controls were made by incubating fixed cells with secondary antibodies only. Coverslips were then fixed on microscope slides and digitized with a cool snap video camera connected to Nikon Eclipse TE200 epifluorescence microscopy (Nikon, Florence, Italy). All images were captured under constant exposure time, gain, and offset. Cell morphology was observed by light microscopy and evaluation of round-shaped cells was performed by direct counting; 100 cells were counted and the average ± SD calculated. Values are given as rounded cell *versus* normal-shaped cells.

RT-PCR. Total RNAs were prepared using TRIzol® Reagent according to the manufacturer's instructions and used for the detection of β-actin and SOD1 mRNAs in semi-quantitative RT-PCR. GAPDH was used as internal control. Briefly, 3 μg total RNA was retrotranscripted in the presence of random primers and M-MLV according to manufacturer's instructions. PCR reactions of β-actin, SOD1 and GAPDH cDNA (35 cycles of 15 s melting at 95°C, 30 s annealing at 55°C, 1 min 20 s extension at 72°C) were performed with Platinum Taq DNA Polymerase (Invitrogen) using the primers listed below:

β-actin-fwd:
5′ ATGGATGATGATATCGCCGCGC 3′;
β-actin-rev:
5′ CTAGAAGCATTTGCGGTGGACG 3′;
SOD1-fwd:
5′ ATGGCGACGAAGGCCGTGTG 3′;
SOD1-rev:
5′ GATCCCAATTACACCACAAGCC 3′;

GAPDH-fwd:
5′ CTCCTCCACCTTTGACGCTG 3′;
GAPDH-rev:
5′ CCACCCTGTTGCTGTAGCCA 3′.
The products obtained were of 1128 bp for β-actin, 495 bp for SOD1 and 100 bp for GAPDH.

Cell fractionation and Western blotting. For determination of total protein content, cell pellets were resuspended in lysis buffer containing 50 mM Tris-HCl, pH 7.4, 150 mM NaCl, 1 % Triton X-100, protease inhibitor cocktail, 40 mM NaF, 1 mM Na_3VO_4. After 30-min incubation on ice, cell lysates were centrifuged at 22 300 *g* for 15 min and the pellet was discarded. To separate the detergent-soluble cytosolic components from the detergent-insoluble cytoskeletal components, cell lysates were separated into Triton-soluble (TS) and Triton-insoluble (TI) fractions according to Xie et al. [24]. Briefly, cell pellets were resuspended in extraction buffer (80 mM MES, pH 6.8, 1 mM $MgCl_2$, 2 mM EGTA, 30 % glycerol, 0.1 % Triton X-100, protease inhibitor cocktail, 40 mM NaF, 1 mM Na_3VO_4) at 37°C for 15 min and then centrifuged at 16 000 *g* for 1 min. Supernatants represented the TS, and pellets (washed two times in Extraction Buffer) the TI fraction. TI pellets were then resuspended in lysis buffer. Nuclei fractions were obtained by cell lysis in NP-40 lysis buffer (NLB) (0.5 % Nonidet P-40, 0.5 M Sucrose, 15 mM TRIS, pH 7.5, 60 mM KCl, 0.25 mM EDTA, 0.125 mM EGTA, 0.5 mM spermine, 0.125 mM spermidine, 50 mM NaF, 1 mM Na_3VO_4, 1 mM DTT) according to Sun et al. [25]. Briefly, cells were resuspended in NLB, incubated on ice for 5 min, and then centrifuged at 600 *g* for 5 min at 4°C. Pellets were washed three times in NLB and then lysed in lysis buffer. Protein content was determined according to Lowry et al. [26]. Protein extracts were resuspended in Laemmli buffer and then electrophoresed on 10 % or 12 % SDS-polyacrylamide gels and blotted onto nitrocellulose. Membranes were stained with primary antibodies against SOD1 (1:2000), Actin (1:5000), α-Tubulin (1:5000), β-Tubulin (1:5000), p38 (1:2000), P-p38 (1:1000), P-MKK3/6 (1:1000), catalase (1:2000), Hsp25 (1:2000), Hsp27 (1:2000), Hsf1 (1:5000), P-Cdk5 (1:500), p35 (1:500) or Tau (1:2000). After incubation with the appropriate HRP-conjugated secondary antibody (1:10 000), protein bands were detected using a Fluorchem Imaging system (Alpha Innotech, San Leandro, CA, USA) after incubation with ChemiGlow chemiluminescence substrate (Alpha Innotech). Density of immunoreactive bands was calculated using the software AlphaEaseFC and normalized for catalase or Ponceau Red staining. For Ponceau Red normalization, we considered the density of all the bands obtained after staining of blotted nitrocellulose membrane.

Determination of SOD1 activity on gel. SOD1 activity was measured on non-denaturing 10 % polyacrylamide gels, by loading 50 μg protein extracts. After electrophoresis, the gel was incubated in NBT solution (2.5 mM) for 30 min in the dark with gentle shaking, followed by 30-min incubation with a solution containing 30 mM tetramethylenediamine and 10 μg/ml riboflavin. SOD1 activity was detected as the achromatic band on the violet-colored gel, obtained after light exposure.

Analysis of apoptosis. Amount of cell death was determined by staining cells with 50 μg/ml propidium iodide (dissolved in 1 mg/ml sodium citrate, 0.1 % Triton X-100) prior cytofluorimetric analysis with FACSCalibur instrument (Becton Dickinson, San Jose, CA, USA). The percentages of apoptotic cells were evaluated according to Nicoletti et al. [27] by using the WinMDI 2.8 software (Scripps Research Institute, La Jolla, CA, USA).

Analysis of superoxide content. Superoxide was detected by cytofluorimetric analysis after incubation for 30 min at 37°C with 5 μM DHE. For cytofluorimetric analysis, cells were scraped, washed, and resuspended in PBS. The fluorescence intensities of 10 000 cells from each sample were acquired by FACSCalibur instrument. Data were analyzed using the WinMDI 2.8 software.

Statistical analysis. The results are presented as means ± SD. Statistical evaluation was conducted by ANOVA, followed by the *post hoc* Student-Newman-Keuls. Differences were considered to be significant at $p<0.05$.

Results

Morphology and F-actin framework of SH-SY5Y cells were altered after SOD1 depletion. We previously demonstrated that SOD1 depletion in neuroblastoma cells efficiently promoted a rapid raise in the intracellular content of superoxide at early times after transfection, when SOD1 content was only moderately affected. We also demonstrated that up-regulation of the antioxidant glutathione was fundamental to buffer intracellular superoxide production and to counteract oxidative damage [23]. Oxidative stress has been largely proposed to have a role in the occurrence of cytoskeleton anomalies. Here we

further analyzed whether the early and transient rise in superoxide due to SOD1 decrease was able to alter cytoskeleton homeostasis. We transiently transfected SH-SY5Y neuroblastoma cells with siRNA against SOD1 (*sisod*) and, as negative control, we used a scrambled sequence matching with no intracellular mRNA (*siscr*). As previously demonstrated, SOD1 deficiency was not associated with the occurrence of cell death [23]. However, as result of SOD1 silencing by RNAi, we observed marked changes in cell morphology at 16 h (Fig. 1A), with the majority of *sisod* cells having a rounded shape, and a reduced extension and number of neurites with respect to *siscr* controls. The percentage of rounded cells accounted for about 80±6%, compatible with the efficiency of transfection. To assess whether alteration in F-actin framework could be responsible for these changes, we carried out microscopic evaluation of the F-actin network upon staining with the fluorescent Alexa Fluor 488-conjugated phalloidin and with anti-SOD1 antibody (as control for SOD1 down-regulation). As expected, Figure 1B shows that, at 16 h after transfection, *sisod* cells showed lower levels of SOD1 with respect to *siscr* and a general impairment of F-actin network. The F-actin appeared disordered and weakened, with a small number of stress fibers especially in those cells with lowest SOD1 content (Fig. 1B). On the other hand, Figure 1B shows that F-actin impairment at 24 h had almost completely recovered, although the decrease of SOD1 content reached a maximum at 48 h, suggesting that the phenomenon was transient and efficiently counteracted by cells. The general lowering and disruption of F-actin framework is also evident in Figure 2A, which shows a higher number of cells stained with phalloidin.

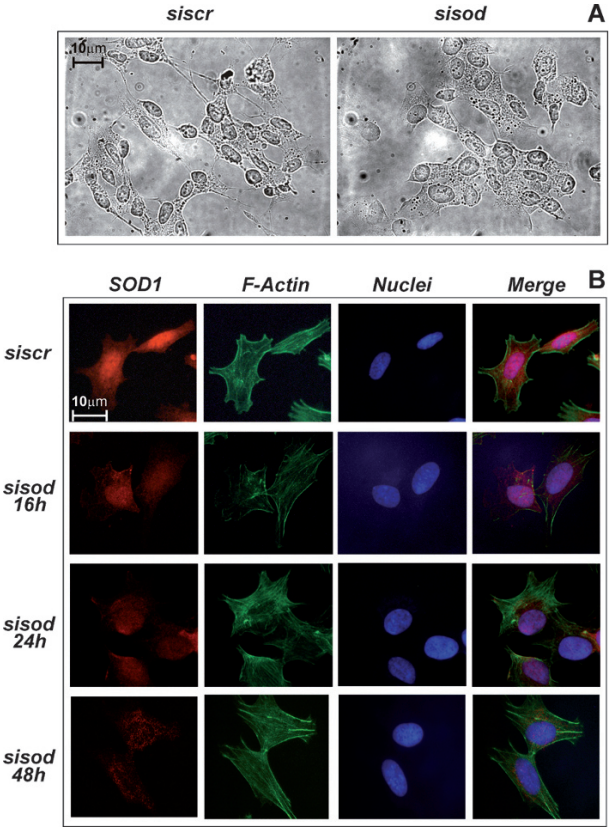

Figure 1. Cu,Zn superoxide dismutase (SOD1) down-regulation induces changes of cell morphology and F-actin network in SH-SY5Y cells. SH-SY5Y cells were transiently transfected with small interference RNA (siRNA) against SOD1 (*sisod*) or with a scramble siRNA (*siscr*). (*A*) After 16 h cells were observed by optic microscopy. (*B*) After 16, 24 and 48 h cells were fixed in paraformaldehyde and stained for fluorescence microscopy analysis with anti-SOD1 antibody (red), Phalloidin-488 (green) to visualize F-actin and Hoechst 33342 to stain nuclei (blue). Images reported are from one experiment representative of five that gave similar results.

Cytoskeletal protein content was affected by SOD1 down-regulation only in neuroblastoma cells. To determine whether the transient changes in cell morphology and F-actin framework could be due to a decrease of actin, we analyzed its content in whole cell lysates by Western blot. Figure 2B shows that at 16 h, although SOD1 protein content was only slightly lowered, actin was highly diminished in *sisod* cells (–61±8%). Notably, at 24 h, actin content returned to value similar to *siscr* cells (data not shown). To verify whether the decrease in actin was due to down-regulation of its expression, we analyzed actin mRNA from *sisod* and *siscr* cells by RT-PCR. Figure 2C shows that no significant changes were detectable in actin RNA content of *sisod* cells with respect to *siscr* at 16 and 24 h after transfection, whereas SOD1 mRNA was highly decreased due to RNAi in *sisod* cells. The data that the high decrease of SOD1 mRNA at 16 h was not paralleled by the same rate of protein reduction confirmed the peculiar stability and long half-life of the protein [28]

We previously demonstrated that the cytoskeletal protein α-tubulin was not affected by SOD1 depletion [23]. Therefore, to assess specificity for actin impairment, we evaluated the content of tubulin in the time frame used in the present work. Figure 2B shows that β-tubulin content was decreased at 16 h after transfection, although at lower extent (–44±7%) with respect to actin, while no changes were detected for α-tubulin.

NFs are intermediate filaments typical of cytoskeleton of cells of neuronal origin and are present in three forms, light (L), medium (M) and heavy (H) chains. To assess whether NFs could be impaired after SOD1 RNAi, we performed Western blot to detect the three forms of NF. Under our experimental conditions, only

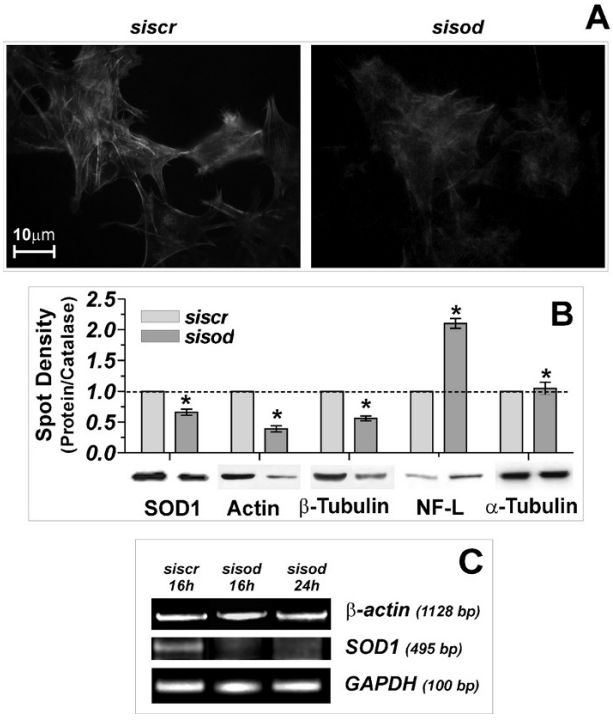

Figure 2. SOD1 down-regulation affects cytoskeletal protein content in SH-SY5Y cells. SH-SY5Y cells were transiently transfected with siRNA against SOD1 (*sisod*) or with a scramble siRNA (*siscr*). (*A*) After 16 h, cells were fixed in paraformaldehyde and stained for fluorescence microscopy analysis with Phalloidin-488 to visualize F-actin. Images reported are from one experiment representative of five that gave similar results. (*B*) After 16 h, SOD1, actin, α- and β-tubulin and neurofilament light chain (NF-L) protein content was determined by Western blot analysis on total protein extracts. All the immunoblots are from one experiment representative of three that gave similar results. Density of immunoreactive bands was calculated using the software AlphaEaseFC and normalized for the respective loading control. Data are expressed as means ± SD; *$p<0.001$, $n=3$. (*C*) β-Actin, SOD1 and GAPDH mRNA content was determined after 16 and 24 h by RT-PCR. The gel reported is representative of three independent experiments that gave similar results.

the NF-L chain was detectable, with the other NF subunits being below the detection limit, in line with the fact that SH-SY5Y are not differentiated cells. Moreover, NF-L levels were significantly raised in *sisod* cells at 16 h after transfection (+110±4 %) (Fig. 2B).

To assess whether cytoskeleton perturbation was typical of this cell type, we extended our studies to other neuroblastoma cell lines such as human CHP100 and mouse NSC34 cells; non-neuronal cell lines such as human gastric adenocarcinoma (AGS) and human melanoma (M14) cells were also examined. NSC34 cells have a multipolar neuron-like phenotype created through the fusion of mouse neuroblastoma N18TG2 with motor neurons derived from spinal cord cells [29]. We focused our attention on actin content, which appeared to be the most affected protein upon SOD1 depletion. Figure 3A shows microscope analysis of NSC34 cells transfected with SOD1 siRNA; in these cells a significant change in cell morphology and a marked decrease in F-actin content at 16 h after SOD1 knock-down were also observed. Western blot analysis of total actin content demonstrated that M14 and AGS cells did not display any change in the actin level at 16 h (Fig. 3B) or at 24 and 48 h (data not shown), while actin was significantly diminished in CHP100 and NSC34 cells at 16 h (Fig. 3B).

F-actin recovery was associated with the up-regulation of Tau and Hsp27. To clarify the molecular mechanisms responsible for the recovery of cytoskeletal network, we separated cell lysates into a TS (containing non-polymerized cytoskeletal proteins) and a TI fraction (containing polymerized cytoskeletal proteins). Actin content was evaluated by Western blot analysis at 16 and 24 h. The immunoblot reported in Figure 4A shows a reduction in actin in the TI fraction (containing F-actin) at 16 h and a recovery of its content at 24 h after transfection, with a decrease in TS fraction (containing G-actin) at 24 h, suggesting that re-polymerization of actin microfilaments was occurring.

Several mechanisms have been proposed to be involved in regulation of F-actin polymerization, among which are included those governed by Tau and Hsp27 proteins. Although the precise role of Tau in cytoskeleton is still controversial, it seems to be responsible for stabilization of F-actin through a cross-linking mechanism [30]. We therefore tested the protein content of Tau at 24 h after transfection, the time at which the recovery of F-actin was found. Total lysates, TS and TI fractions were analyzed by Western blot using an antibody capable of also recognizing phosphorylated forms of Tau. Figure 4B shows that, although no conspicuous variations in phosphorylation levels were observed, the concentration of Tau in *sisod* cells was significantly increased in total, TI and TS fractions. In particular, the accumulation of Tau was mainly evident in TI fraction. An additional band was detected in the TS fraction at higher molecular weight that likely corresponded to its phosphorylated form.

Various injuries and regeneration stimuli are followed by up-regulation of the small heat shock protein Hsp27, which can also represent an actin polymerization modulator. Hsp27 is an actin (+)-end binding protein inhibiting F-actin polymerization and responsible for the delay of cell cycle [31]. Subsequent dissociation of Hsp27 from F-actin reactivates microfilament growth [32]. To assess whether Hsp27 is involved in the alterations of cytoskeleton induced by SOD1 depletion, we analyzed total concentration of

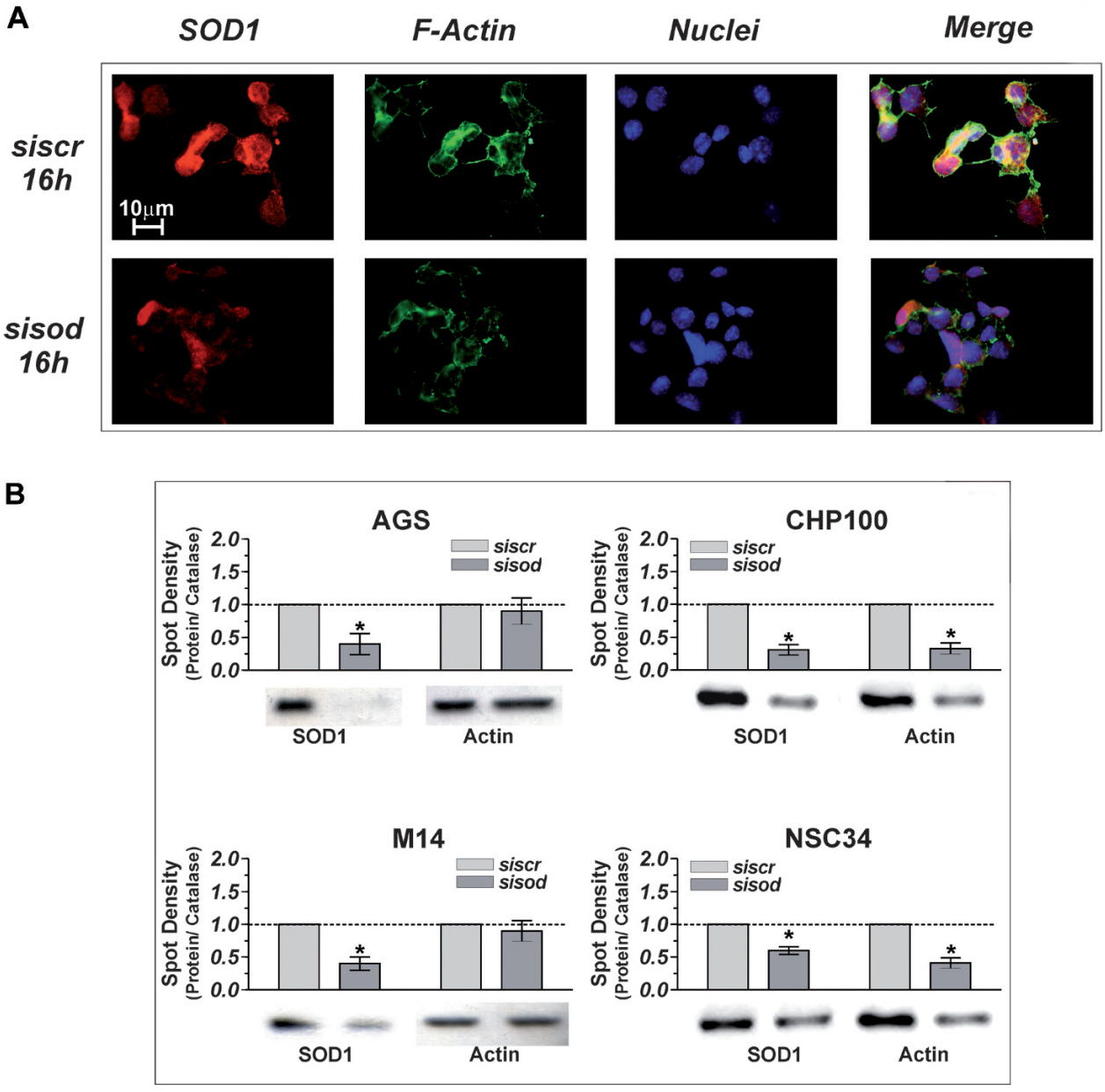

Figure 3. SOD1 down-regulation affects cytoskeletal protein content in neuroblastoma cells. (*A*) NSC34 cells were transiently transfected with siRNA against SOD1 (*sisod*) or with a scramble siRNA (*siscr*); after 16 h, cells were fixed in paraformaldehyde and stained with anti-SOD1 antibody (red), Phalloidin-488 (green) to stain F-actin and Hoechst 33342 to stain nuclei (blue) and observed by fluorescence microscopy. (*B*) AGS, M14, CHP100 and NSC34 cells were transiently transfected with siRNA against SOD1 (*sisod*) or with a scramble siRNA (*siscr*). Actin protein content was determined by Western blot analysis on total protein extracts at 16 h after transfection. All the immunoblots are from one experiment representative of three that gave similar results. Density of immunoreactive bands was calculated using the software AlphaEaseFC and normalized for the respective loading control. Data are expressed as means ± SD; *$p<0.001$, $n=3$.

Hsp27 by Western blot. Figure 4C shows that Hsp27 content was highly elevated in *sisod* cells at 16 h. The increase of this small heat shock protein was also confirmed in NSC34 cells, which express the murine homologous Hsp25 (Fig. 4C). To evaluate whether Hsp27 accumulation could change the polymerization status of actin, we separated cell lysates in TS and TI fractions, and examined Hsp27 localization and content by Western blot. Figure 4D shows that Hsp27 in *sisod* cells was mainly localized in TI fraction at 16 h and then translocated in TS fraction at 24 h after transfection.

Activation of p38 MAPK was involved in the prevention of cell death. It has been demonstrated that the activation of p38/Hsp27 pathway is an important modulator of actin reorganization after oxidative stress [14]. Moreover, the association of the murine

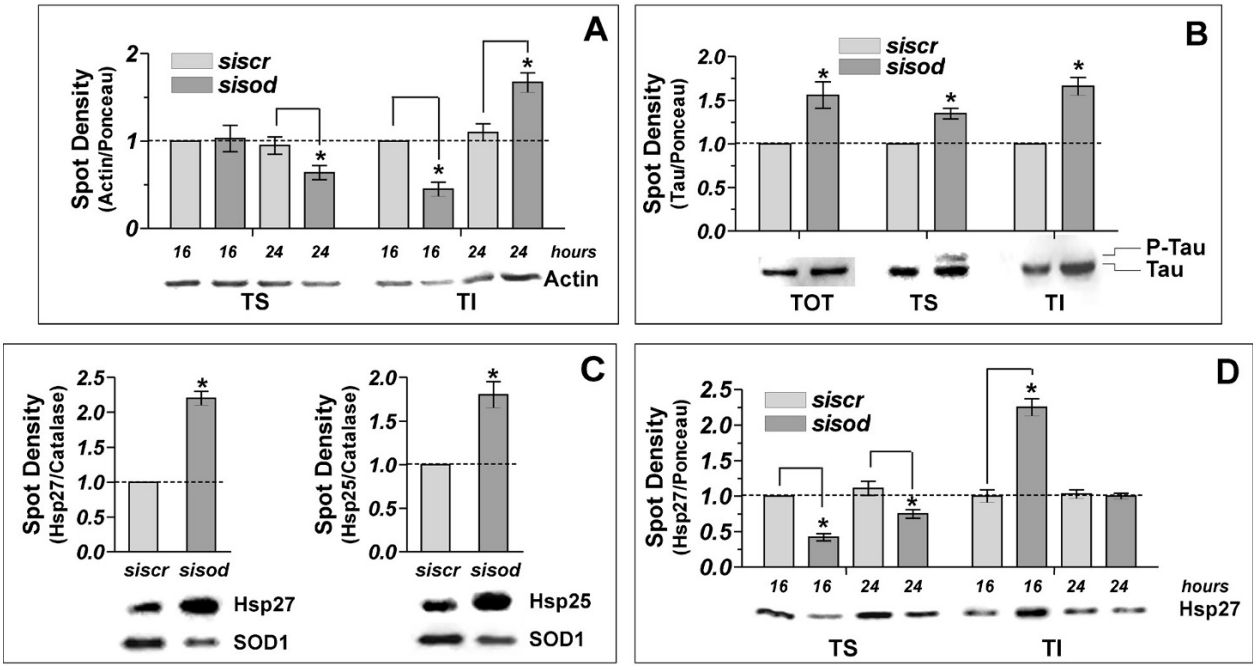

Figure 4. Actin localization, Tau and Hsp27 content are modulated after SOD1 RNA interference (RNAi). SH-SY5Y cells and NSC34 cells were transiently transfected with siRNA against SOD1 (*sisod*) or with a scramble siRNA (*siscr*). (*A*) Actin protein content was determined by Western blot analysis, at 16 and 24 h after transfection, on Triton-soluble (TS) and Triton-insoluble (TI) protein fractions from SH-SY5Y. (*B*) Tau content was determined at 16 h after transfection by Western blot analysis in total, TS and TI extracts protein fractions from SH-SY5Y. (*C*) SOD1, Hsp27 and Hsp25 protein content was determined at 16 h by Western blot analysis on total protein extracts from SH-SY5Y and NSC34 cells, respectively. (*D*) Hsp27 protein content was determined at 16 and 24 h after transfection in TS and TI protein fractions from SH-SY5Y cells. Immunoblots reported are from one experiment representative of three that gave similar results. Density of immunoreactive bands was calculated using the software AlphaEaseFC and normalized for the respective loading control. Data are expressed as means ± SD; *$p<0.001$, $n=3$.

homologue Hsp25 with microfilaments was abolished by the induction of p38/MAPK, thus allowing microfilament growth and cell survival [32]. To assess whether changes of Hsp27 localization could be associated with the activation of p38/MAPK, we analyzed the content of p38, its phospho-active form (P-p38) and its upstream kinase MKK3/6 by Western blot. Figure 5A shows that total p38 protein level did not change during the time course observed. In contrast, significant increase of P-p38 was noticeable at 16 h (+70±6 %) with a peak at 24 h (+570±15 %). Moreover, the levels of phospho-active MKK3/6 were also increased at 16 h (+280±13 %), demonstrating the effective activation of this pathway.

After oxidative stress, Hsp27 is up-regulated *via* the activation of the transcription factor Hsf1, as a cellular protective response [33]. To verify whether Hsf1 could be responsible for Hsp27 up-regulation, we monitored its content in total cell lysates and nuclei by Western blot. Figure 5B shows that in *sisod* cells at 16 and 24 h a significant portion of Hsf1 translocated into the nucleus with a concomitant decrease of its cytosolic counterpart, suggesting its activation. It has been demonstrated that p38 activation could be responsible for nuclear translocation of Hsf1 [34, 35]. Therefore, to verify whether p38 phosphorylation was an upstream event of Hsf1 translocation, immediately after transfection we treated the cells with 20 μM SB203580, a specific inhibitor of p38 phosphorylation. As shown in Figure 5B, Hsf1 failed to translocate into the nucleus after SB203580 treatment, as the nuclear level of Hsf1 in *sisod* cells was comparable with that of *siscr*, even though its content in cytoplasmic fraction was increased. To verify whether p38 activation was necessary for cell survival, we treated *siscr* and *sisod* cells with SB203580 and analyzed the effects on cell viability by cytofluorimetric analysis after propidium iodide staining. According to Nicoletti et al. [36], the appearance of a distinct sub-G1 cell population indicated the occurrence of apoptotic cell death (data not shown). Figure 5C shows that apoptosis was significantly higher in *sisod* cells at 24 and 48 h after transfection with respect to *siscr* cells.

Cdk5/p35 system was activated upon SOD1 deficiency. As reported above, we demonstrated that the cytoskeletal perturbation was specific for neuroblastoma cells. This phenomenon suggested the involvement of molecular pathways that are peculiar of neuronal cell lines. Among the pathways regulating

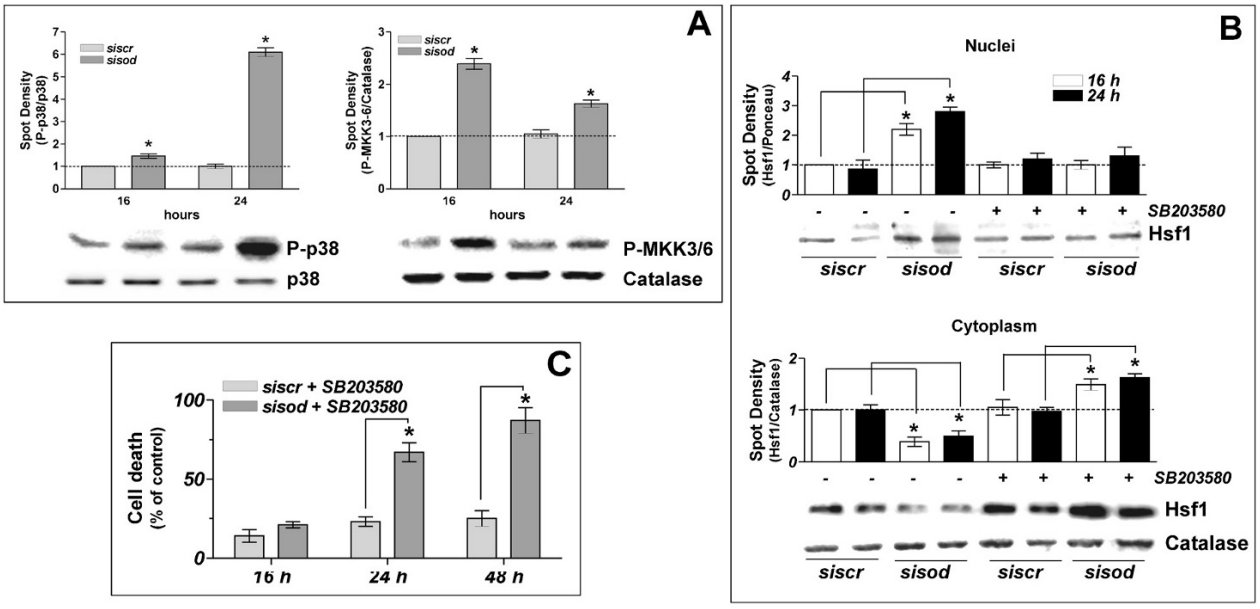

Figure 5. Activation of p38 MAPK mediates cell survival after SOD1 RNAi. SH-SY5Y cells were transiently transfected with siRNA against SOD1 (*sisod*) or with a scramble siRNA (*siscr*). (*A*) p38, P-p38 and P-MKK3/6 protein content was determined 16 and 24 h after transfection by Western blot in total protein extracts. (*B*) Immediately after transfection, cells were treated with 20 μM p38 inhibitor SB203580. After 16 and 24 h, Hsf1 protein content was determined by Western blot analysis in cytoplasmic and nuclear protein fractions. All the immunoblots reported are from one experiment representative of three that gave similar results. Density of immunoreactive bands was calculated using the software AlphaEaseFC and normalized for the respective loading control. Data are expressed as means ± SD; $*p<0.001$, $n=3$. (*C*) Cell death was determined by cytofluorimetric analysis after propidium iodide staining of *siscr* and *sisod* cells treated or not with 20 μM p38 inhibitor SB203580. Analysis of cell death was performed by a FACSCalibur instrument and percentages of cells were calculated using the WinMDI 2.8 software. Data are represented as percentage of control, which corresponds to untreated SB203580 cells and expressed as means ± SD; $*p<0.001$, $n=5$.

actin dynamics, a good candidate could be that mediated by Cdk5/p35 [37, 38]. Cdk5 can be an oxidative stress-regulated kinase, which is activated by the interaction with the neuron-specific regulatory protein p35 [39]. Thus, we examined Cdk5/p35 pathway in our experimental system. As shown in Figure 6A, Western blot analysis, using an antibody specific for the phospho-active form of Cdk5, demonstrated that it increased up to 24 h to finally return to almost basal level at 48 h. p35 was also rapidly accumulated in *sisod* cells at early times and its levels then decreased at 48 h after transfection, mirroring the trend of P-Cdk5. Moreover, we found that this behavior paralleled the burst of superoxide due to SOD1 protein (Fig. 6B) and activity decrease (Fig. 6C), suggesting that ROS burst could be the primary inducer of the processes observed.

Transient superoxide increase is responsible for F-actin depolymerization and activation of Cdk5/p35 pathway. To demonstrate whether the effects on cytoskeletal proteins and on the activation of cytoskeletal-regulatory pathways were all mediated by a burst of superoxide or whether the responses were somehow directly related to SOD1 silencing, we performed experiments in the presence of the anti-oxidant agent NAC. Firstly, to evaluate whether the phenomenon of F-actin depolymerization, elicited by SOD1 silencing, was prevented by NAC, SH-SY5Y cells were transfected with *siscr* and *sisod* sequences and immediately treated with 5 mM NAC for 16 or 24 h. Figure 7A shows that after treatment with NAC, F-actin depolymerization was efficiently prevented at all time points tested. To verify whether P-Cdk5/p35 was up-regulated as consequence of superoxide burst, we analyzed their content in cell lysates by Western blot. As shown in Figure 7B, both at 16 and 24 h after transfection, the rise in p35 level as well as the activation of Cdk5 was inhibited by NAC treatment. These data clearly suggested that transient superoxide increase occurring after SOD1 deficiency was responsible for the events finally leading to cytoskeleton disruption.

Discussion

Previous work from our laboratory demonstrated that the depletion of SOD1 in neuroblastoma cells induced by RNAi gave rise to an early burst of ROS flux that resulted in specific oxidative mitochondrial damage without inducing cell death [23]. This

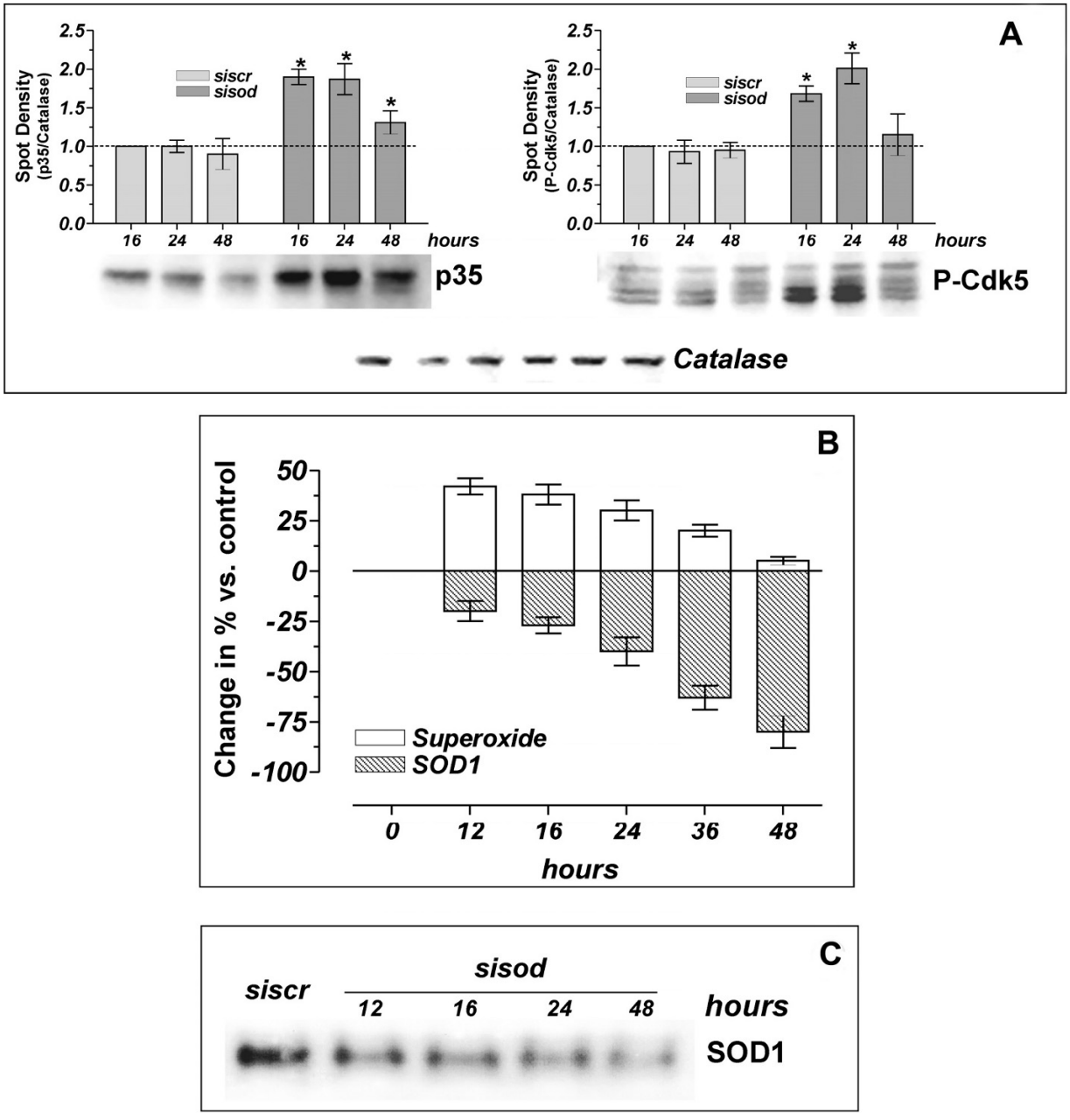

Figure 6. SOD1 down-regulation induces up-regulation of p35 and P-Cdk5. SH-SY5Y cells were transiently transfected with siRNA against SOD1 (*sisod*) or with a scramble siRNA (*siscr*). (*A*) At 16, 24 and 48 h after transfection, P-Cdk5 and p35 protein content was determined by Western blot analysis in total protein extracts; immunoblots reported are from one experiment representative of three which gave similar results. Density of immunoreactive bands was calculated using the software AlphaEaseFC and normalized for the respective loading control. Data are expressed as means ± SD; *$p<0.001$, $n=3$. (*B*) At 12, 24, 36 and 48 h after SH-SY5Y transfection, superoxide content was determined by cytofluorimetric analysis after staining with dihydroethydium. At the same time points, SOD1 protein content was determined by Western blot in total protein extracts; density of immunoreactive bands was calculated using the software AlphaEaseFC and normalized for the loading control. Data are expressed as means ± SD; *$p<0.001$, $n=3$. (*C*) At 12, 16, 24 and 48 h after transfection, cell lysates were separated by native PAGE, and gel stained for SOD1 activity. The negative image of one gel representative of three from independent experiments that gave similar results is shown.

phenomenon has broad potential implications in relation to the role played by SOD1 in diseases associated with oxidative redox perturbations and represents a model of sensitization to the harmful impairment of SOD1. Using the same model, in the present report we found that, besides mitochondrial impairment, cytoskeleton and its regulating redox-sensitive signaling pathways were also altered as consequence of superoxide unbalance caused by SOD1 decrease. In particular, we demonstrated that,

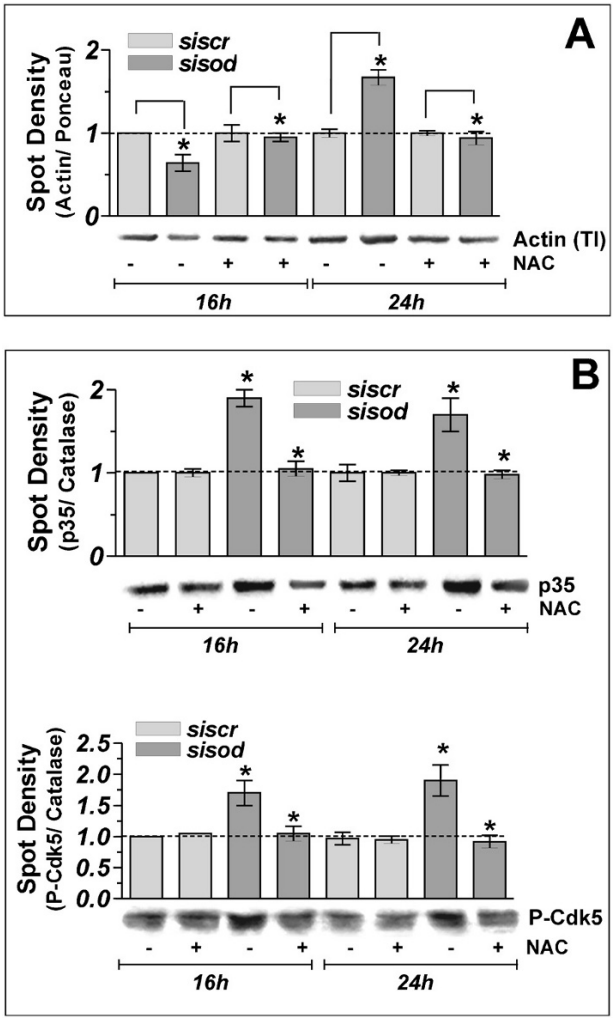

Figure 7. Actin depolymerization and P-Cdk5/p35 activation are a consequence of redox unbalance. SH-SY5Y cells were transiently transfected with siRNA against SOD1 (*sisod*) or with a scramble siRNA (*siscr*). Immediately after transfection 5 mM *N*-acetyl-L-cysteine (NAC) was added to cell culture medium, and cultures were maintained for the next 16 or 24 h. (*A*) Actin protein content was determined by Western blot analysis on the TI protein fraction. (*B*) P-Cdk5 and p35 protein content was determined by Western blot analysis in total protein extracts. Immunoblots reported are from one experiment representative of three that gave similar results. Density of immunoreactive bands was calculated using the software AlphaEaseFC and normalized for the respective loading control. Data are expressed as means ± SD; *$p<0.001$, $n=3$.

at early stages of SOD1 depletion in neuroblastoma cells, an alteration of cells morphology due to a decrease in actin occurred, together with the alteration in the content of other cytoskeletal proteins. Cytoskeletal disturbance was mainly due to actin and β-tubulin decrease and increase of intermediate filaments NF-L. Both in our previous work and here we noticed that, upon SOD1 deficiency, the α isoform of tubulin did not undergo any change in its protein content; this phenomenon is in agreement with data from literature in which a preferential susceptibility of β-tubulin to oxidative unbalance has been reported. Specifically, it has been demonstrated that β-tubulin, but not the heterodimeric counterpart α-tubulin, can be oxidized on methionine [5] and cysteine residues [4]. Oxidative modifications are also effective on actin, in which cysteine and methionine residues can be oxidatively modified [3] and seem to represent sensors of oxidative stress at least in yeasts [40].

It was previously reported that SOD1 could directly interact with microfilaments (through anchorage at dynein heavy chain and actin) [22, 41], suggesting a role in the maintenance of cytoskeleton in terms of direct participation in cytoskeleton architecture and/or local protection against physiologically produced superoxide. Using NAC treatment, we demonstrated that SOD1 protected actin by preventing superoxide-mediated damage. There are at least three different possibilities to explain superoxide-mediated total actin depletion, *i.e.*, degradative mechanisms, decrease of its expression, or occurrence of oxidative modifications (*e.g.*, S-glutathiolation, carbonylation, nitrosylation) masking the epitopes necessary for antibody detection. RT-PCR analysis demonstrated that, during the depolymerization and the following F-actin repolymerization, mRNA content did not change, suggesting that its expression was not affected. The hypothesis that the actin epitopes recognized by the monoclonal antibody used could be masked was excluded, as the use of other antibodies (rabbit and goat polyclonals) gave the same results (data not shown). Finally, proteolysis-derived bands (*e.g.*, those derived by calpains or caspases cleavage) were not detectable under our experimental conditions. However, we cannot exclude that total actin (and also β-tubulin) depletion could be due to intracellular degradative processes.

It is known that the up-regulation of Hsp27 occurs as a response to ROS-mediated microfilament disruption and is protective against apoptosis [14]. Hsp27 protein, as well as the actin stabilizing agent phalloidin, has been demonstrated to delay cytochrome c release and caspase activation under pro-apoptotic stimuli [42]. Moreover, Hsp27 inhibits actin polymerization by linking to growing ends of F-actin. According to literature, activation of p38 may be responsible for the release of Hsp27 from cytoskeleton, thus switching-off its inhibitory effect on actin polymerization, and the recovery of cell shape and survival. This was confirmed under our experimental conditions in which, under SOD1 deficiency, we at first found a strong up-regulation of Hsp27 concomitantly with the loss of F-actin. Separation of cell lysates into TS and TI fractions showed that Hsp27 was initially localized in cytoskeleton and finally

detached from F-actin, thus translocating into the cytosol. Furthermore, the MKK3/6-dependent activation of p38 pathway was also effective under SOD1 deficiency and its activation is essential for preventing cell death. Experiment carried out in the presence of the inhibitor of p38 SB203580 demonstrated that p38 activity was essential for Hsf1 translocation into the nucleus and for cell survival after SOD1-mediated cytoskeleton impairment. Therefore, we suggest that assuring a rapid recovery of cytoskeleton from its transient deregulation might be the key factor for the choice between cell death and survival. In addition, we demonstrated the activation of the Cdk5/p35 system, which represents a ROS-sensitive pathway that is an important modulator of cytoskeletal dynamics in cells of neuronal origin [37, 43–46]. As reported, SOD1 depletion after RNAi induced an early up-regulation of superoxide giving rise to mild oxidative stress that was then rapidly buffered by GSH increase [23]. The results obtained in the present work on the phospho-mediated activation of Cdk5 at early time points match well with the rise of superoxide level and its successive buffering. In particular, the P-Cdk5 trend mirrored that of GSH, suggesting that this antioxidant could be able and sufficient to switch-off superoxide-mediated Cdk5/p35 activation. Experiments carried out in the presence of NAC further confirmed that redox unbalance was responsible for the activation of this pathway and of the downstream effects. We also demonstrated the accumulation of Cdk5 regulatory subunit p35, but not of its cleavage product p25. This result is in line with the notion that p35 accumulates under mild oxidative stress and is cleaved into the p25 product only after a prolonged and sustained oxidative insult [15, 16]. Cdk5 is a proline-directed kinase that phosphorylates serines and threonines in NFs and microtubule subunits. Binding of p35 to Cdk5 is sufficient for activation and modulation of cytoskeletal neuronal proteins such as Tau and NF [45, 46]. The active Cdk5/p35 complex has been found to also influence actin behavior through modulation of the Rac effector, p21-activated kinase1 (Pak1) [47]. Compatible with transient activation of Cdk5, we found a significant accumulation of both NF-L and Tau proteins and a detectable increase of phosphorylated form of Tau.

The phenomenon of cytoskeleton impairment associated with SOD1 deficiency seemed to be effective only in the neuroblastoma cells screened (SH-SY5Y, NSC34, CHP100), in line with the notion that neuron-derived cells are particularly susceptible to oxidative unbalance [48]. In contrast, under the same experimental conditions, melanoma M14 and adenocarcinoma AGS cells did not undergo superoxide unbalance and actin depletion. This evidence is in line with data from our previous work in which we demonstrated that AGS cells can promptly counteract oxidative stress due to their efficient antioxidant defense system [49].

Overall data evidenced that SOD1 down-regulation in proliferating cells of neural origin leads to a breakdown of the cytoskeletal framework, which is related to the superoxide-mediated increase of Cdk5 activity. It has been reported that F-actin directly links to mitochondrial voltage-dependent anion channels (VDAC), regulating, together with Bcl-2, their gating [27]. For this reason, the data obtained in this work could explain, at least in part, the impairment of mitochondrial transmembrane potential seen as late effect of SOD1 deficiency [23]. The present data reveal a novel point of view in understanding the importance of SOD1 antioxidant activity in the maintenance of neuroblastoma cytoskeleton, being a switch for Cdk5/p35 activation. Our data may contribute to clarifying the role of p38/Hsp27 pathway in the recovery of the microfilament framework under mild oxidative stress conditions, and suggest an implication of SOD1 in the onset of diseases (*e.g.*, aging and neurodegeneration) in which both the loss of cytoskeletal integrity and oxidative stress have been largely reported. Moreover, our data confirm the peculiar sensitivity of cytoskeleton of cells of neuronal origin to oxidative stress [48] and demonstrate that these cells are provided with efficient recovery systems able to prevent cell death. Finally, our findings could also be useful in suggesting new strategies in treatment of neuroblastomas, such as the combined use of redox chemotherapeutic agents with p38 inhibitors.

Acknowledgements. This work was partially supported by grants from Ministero della Salute and MIUR, FIRB "Idee progettuali".

1 Dalle Donne, I., Rossi, R., Milzani, A., Di Simplicio, P. and Colombo, R. (2001) The actin cytoskeleton response to oxidants: From small heat shock protein phosphorylation to changes in the redox state of actin itself. Free Radic. Biol. Med. 31, 1624–1632.

2 Askenov, M. Y., Aksenova, M. V., Butterfield, D. A., Geddes, J. W. and Markesbery, W. R. (2001) Protein oxidation in the brain in Alzheimer's disease. Neuroscience 103, 373–383.

3 Dalle-Donne, I., Rossi, R., Giustarini, D., Gagliano, N., Di Simplicio, P., Colombo, R. and Milzani, A. (2002) Methionine oxidation as a major cause of the functional impairment of oxidized actin Free Radic. Biol. Med. 32, 927–937.

4 Hosono, T., Fukao, T., Ogihara, J., Ito Y., Shiba, H., Seki, T. and Ariga, T. (2005) Diallyl trisulfide suppresses the proliferation and induces apoptosis of human colon cancer cells through oxidative modification of beta-tubulin. J. Biol. Chem. 280, 41487–41493.

5 Boutte, A. M., Woltjer, R. L., Zimmerman, L. J., Stamer, S. L., Montine, K. S., Manno, M. V., Cimino, P. J., Liebler, D. C. and Montine, T. J. (2006) Selectively increased oxidative modifications mapped to detergent-insoluble forms of Aβ and β-III tubulin in Alzheimer's disease. FASEB J. 20, 1473–1483.

6 Niewiadomska, G., Baksalerska-Pazera, M. and Riedel, G. (2006) Cytoskeletal transport in the aging brain: Focus on the cholinergic system. Rev. Neurosci. 17, 581–618.

7 Kang, K. W., Lee, S. J. and Kim, S. G. (2005) Molecular mechanism of Nrf2 activation by oxidative stress. Antioxid. Redox Signal. 7, 1664–1673.

8 Mirabelli, F., Salis, A., Perotti, M., Taddei, F., Bellomo, G. and Orrenius, S. (1988) Alterations of surface morphology caused by the metabolism of menadione in mammalian cells are associated with the oxidation of critical sulfhydryl groups in cytoskeletal proteins. Biochem. Pharmacol. 37, 3423–3427.

9 Rokutan, K., Johnston, R. B. Jr. and Kawai, K. (1994) Oxidative stress induces S-thiolation of specific proteins in cultured gastric mucosal cells. Am. J. Physiol. 266, G247–G254.

10 Caprari, P., Bozzi, A., Malorni, W., Bottini, A., Iosi F., Santini, M. T. and Salvati, A. M. (1995) Junctional sites of erythrocyte skeletal proteins are specific targets of tert-butylhydroperoxide oxidative damage. Chem. Biol. Interact. 94, 243–258.

11 Banan, A., Fitzpatrick, L., Zhang, Y. and Keshavarzian, A. (2001) OPC compounds prevent oxidant-induced carbonylation and depolymerization of the F-actin cytoskeleton and intestinal barrier hyperpermeability. Free Radic. Biol. Med. 30, 287–298.

12 Dourdin, N., Bhatt, A. K., Dutt, P., Greer, P. A., Arthur, J. S., Elce, J. S. and Huttenlocher, A. (2001) Reduced cell migration and disruption of the actin cytoskeleton in calpain-deficient embryonic fibroblasts. J. Biol. Chem. 276, 48382–48388.

13 Huot, J., Houle, F., Spitz, D. R. and Landry, J. (1996) HSP27 phosphorylation-mediated resistance against actin fragmentation and cell death induced by oxidative stress. Cancer Res. 56, 273–279.

14 Huot, J., Houle, F., Marceau, F. and Landry, J. (1997) Oxidative stress-induced actin reorganization mediated by the p38 mitogen-activated protein kinase/heat shock protein 27 pathway in vascular endothelial cells. Circ. Res. 80, 383–392.

15 Dhavan, R. and Tsai, L. H. (2001) A decade of CDK5. Nat. Rev. Mol. Cell Biol. 2, 749–759.

16 Sahlgren, C. M., Pallari, H. M., He, T., Chou, Y. H., Goldman, R. D. and Eriksson, J. E. (2006) A nestin scaffold links Cdk5/p35 signaling to oxidant-induced cell death. EMBO J. 25, 4808–4819.

17 Nimnual, A. S., Taylor, L. J. and Bar-Sagi, D. (2003) Redox-dependent downregulation of Rho by Rac. Nat. Cell Biol. 5, 236–241.

18 Halliwell, B. (2006) oxidative stress and eurodegeneration: Where are we now? J. Neurochem. 97, 1634–1658.

19 Hensley, K., Robinson, K. A., Gabbita, S. P., Salsman, S. and Floyd, R. A. (2000) Reactive oxygen species, cell signaling, and cell injury. Free Radic. Biol. Med. 28, 1456–1462.

20 Furukawa, Y. and O'Halloran, T. V. (2006) Posttranslational modifications in Cu,Zn-superoxide dismutase and mutations associated with amyotrophic lateral sclerosis. Antioxid. Redox Signal. 8, 847–867.

21 Pasinelli, P., Belford, M. E., Lennon, N., Bacskai, B. J., Hyman, B. T., Trotti, D. and Brown, R. H. Jr. (2004) Amyotrophic lateral sclerosis-associated SOD1 mutant proteins bind and aggregate with Bcl-2 in spinal cord mitochondria. Neuron 43, 19–30.

22 Takamiya, R., Takahashi, M., Park, Y. S., Tawara, Y., Fujiwara, N., Miyamoto, Y., Gu, J., Suzuki, K. and Taniguchi, N. (2005) Overexpression of mutated Cu,Zn-SOD in neuroblastoma cells results in cytoskeletal change. Am. J. Physiol. Cell Physiol. 288, 253–259.

23 Aquilano, K., Vigilanza, P., Rotilio, G. and Ciriolo, M. R. (2006) Mitochondrial damage due to SOD1 deficiency in SH-SY5Y neuroblastoma cells: A rationale for the redundancy of SOD1. FASEB J. 20, 1683–1685.

24 Xie, H., Litersky, J. M., Hartigan, J. A., Jope, R. S. and Johnson, G. V. (1998) The interrelationship between selective tau phosphorylation and microtubule association. Brain Res. 798, 173–183.

25 Sun, F. C., Wei, S., Li, C. W., Chang, Y. S., Chao, C. C. and Lai, Y. K. (2006) Localization of GRP78 to mitochondria under the unfolded protein response. Biochem. J. 396, 31–39.

26 Lowry, O. H., Rosebrough, N. J., Farr, A. L. and Randall, R. J. (1951) Protein measurement with the Folin phenol reagent. J. Biol. Chem. 193, 265–275.

27 Tsujimoto, Y. (2002) Bcl-2 family of proteins: Life-or-death switch in mitochondria. Biosci. Rep. 22, 47–58.

28 Bartnikas, T. B. and Gitlin, J. D. (2003) Mechanisms of biosynthesis of mammalian copper/zinc superoxide dismutase. J. Biol. Chem. 278, 33602–33608.

29 Cashman, N. R., Durham, H. D., Blusztajn, J. K., Oda, K., Tabira, T., Shaw, I. T., Dahrouge, S. and Antel, J. P. (1992) Neuroblastoma x spinal cord (NSC) hybrid cell lines resemble developing motor neurons. Dev. Dyn. 194, 209–221.

30 Fulga, T. A., Elson-Schwab, I., Khurana, V., Steinhilb, M. L., Spires, T. L., Hyman, B. T. and Feany, M. B. (2007) Abnormal bundling and accumulation of F-actin mediates tau-induced neuronal degeneration *in vivo*. Nat. Cell Biol. 9, 139–148.

31 Lee, J. H., Sun, D., Cho, K. J., Kim, M. S., Hong, M. H., Kim, I. K., Lee, J. S. and Lee, J. H. (2007) Overexpression of human 27 kDa heat shock protein in laryngeal cancer cells confers chemoresistance associated with cell growth delay. J. Cancer Res. Clin. Oncol. 133, 37–46.

32 Murashov, A. K., Ul Haq, I., Hill, C., Park, E., Smith, M., Wang, X., Wang, X., Goldberg D. J. and Wolgemuth D. J. (2001) Crosstalk between p38, Hsp25 and Akt in spinal motor neurons after sciatic nerve injury. Brain Res. Mol. Brain Res. 93, 199–208.

33 Filomeni, G., Aquilano, K., Rotilio, G. and Ciriolo, M. R. (2005) Antiapoptotic response to induced GSH depletion: Involvement of heat shock proteins and NF-kappaB activation. Antioxid. Redox Signal. 7, 446–55.

34 Hung, J. J., Cheng, T. J., Lai, Y. K. and Chang, M. D. (1998) Differential activation of p38 mitogen-activated protein kinase and extracellular signal-regulated protein kinases confers cadmium-induced HSP70 expression in 9L rat brain tumor cells. J. Biol. Chem. 273, 31924–31931.

35 Rafiee, P., Theriot, M. E., Nelson, V. M., Heidemann, J., Kanaa, Y., Horowitz, S. A., Rogaczewski, A., Johnson, C. P., Ali, I., Shaker, R. and Binion, D. G. (2006) Human esophageal microvascular endothelial cells respond to acidic pH stress by PI3K/AKT and p38 MAPK-regulated induction of Hsp70 and Hsp27. Am. J. Physiol. Cell Physiol. 291, C931–945.

36 Nicoletti, I., Migliorati, G., Pagliacci, M. C., Grignani, F. and Riccardi, C. (1991) A rapid and simple method for measuring thymocyte apoptosis by propidium iodide staining and flow cytometry. J. Immunol. Methods 139, 271–279.

37 Patrick, G. N., Zhou, P., Kwon, Y. T., Howley, P. M. and Tsai, L. H. (1998) p35, the neuronal-specific activator of cyclin-dependent kinase 5 (Cdk5) is degraded by the ubiquitin-proteasome pathway. J. Biol. Chem. 273, 24057–24064.

38 Patrick, G. N., Zukerberg, L., Nikolic, M., de la Monte, S., Dikkes, P. and Tsai, L. H. (1999) Conversion of p35 to p25 deregulates Cdk5 activity and promotes neurodegeneration. Nature 402, 615–622.

39 Strocchi, P., Pession, A. and Dozza, B. (2003) Up-regulation of cDK5/p35 by oxidative stress in human neuroblastoma IMR-32 cells. J. Cell. Biochem. 88, 758–765.

40 Farah, M. E. and Amberg, D. C. (2007) Conserved actin cysteine residues are oxidative stress sensors that can regulate cell death in yeast. Mol. Biol. Cell. 18, 1359–1369.

41 Zhang, F., Ström, A. L., Fukada, K., Lee, S., Hayward, L. J. and Zhu, H. (2007) Interaction between familial amyotrophic lateral sclerosis (ALS)-linked SOD1 mutants and the dynein complex. J. Biol. Chem. 282, 16691–16699.

42 Paul, C., Manero, F., Gonin, S., Kretz-Remy, C., Virot, S. and Arrigo, A. P. (2002) Hsp27 as a negative regulator of cytochrome C release. Mol. Cell. Biol. 22, 816–834.

43 Maccioni, R. B., Otth, C., Concha, I. I. and Muñoz, J. P. (2001) The protein kinase Cdk5. Structural aspects, roles in neuro-

genesis and involvement in Alzheimer's pathology. Eur. J. Biochem. 268, 1518–1527.
44 Shea, T. B., Zheng, Y. L., Ortiz, D. and Pant, H. C. (2004) Cyclin-dependent kinase 5 increases perikaryal neurofilament phosphorylation and inhibits neurofilament axonal transport in response to oxidative stress. J. Neurosci. Res. 76, 795–800.
45 Tsai, L. H., Delalle, I., Caviness, V. S. Jr., Chae, T. and Harlow, E. (1994) p35 is a neural-specific regulatory subunit of cyclin-dependent kinase 5. Nature 371, 419–423.
46 Ishiguro, K., Kobayashi, S., Omori, A., Takamatsu, M., Yonekura, S., Anzai, K., Imahori, K. and Uchida, T. (1994) Identification of the 23 kDa subunit of tau protein kinase II as a putative activator of cdk5 in bovine brain. FEBS Lett. 342, 203–208.
47 Edwards, D. C., Sanders, L. C., Bokoch, G. M. and Gill, G. N. (1999) Activation of LIM-kinase by Pak1 couples Rac/Cdc42 GTPase signalling to actin cytoskeletal dynamics. Nat. Cell Biol. 1, 253–259.
48 Mattson, M. P. and Magnus, T. (2006) Ageing and neuronal vulnerability. Nat. Rev. Neurosci. 7, 278–294.
49 Filomeni, G., Aquilano, K., Rotilio, G. and Ciriolo, M. R. (2005) Glutathione-related systems and modulation of extracellular signal-regulated kinases are involved in the resistance of AGS adenocarcinoma gastric cells to diallyl disulfide-induced apoptosis. Cancer Res. 65, 11735–11742.